ACS OMEGA

Open Access

http://pubs.acs.org/journal/acsodf

Article

Electron Irradiation-Induced Degradation of TiN Thin Films on Quartz and Sapphire Substrates

Gulnur Akhtanova, Yerassyl Yerlanuly, Hryhorii P. Parkhomenko, Mykhailo V. Solovan, Andrii I. Mostovyi, Aliya K. Nurmukhanbetova, Alexander V. Kireyev, Igor V. Danko, Pavel A. Oreshkin, Timur K. Zholdybayev, Daniyar M. Janseitov, Tlekkabul S. Ramazanov, and Viktor V. Brus*

Cite This: *ACS Omega* 2024, 9, 925−933

Read Online

ACCESS | Metrics & More | Article Recommendations | Supporting Information

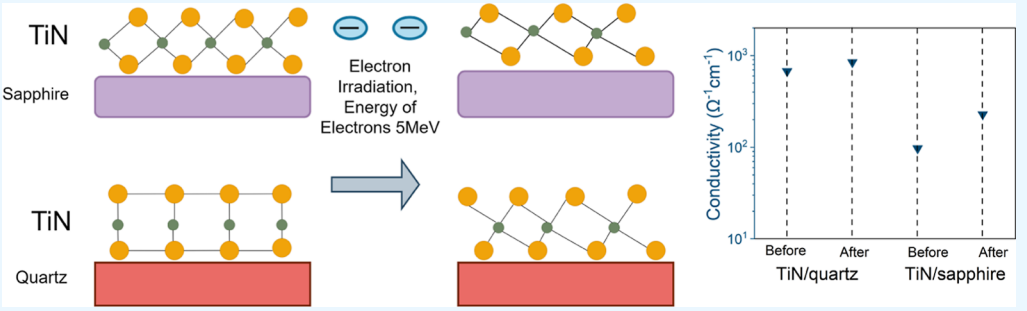

ABSTRACT: In this contribution, we investigated the properties of magnetron-sputtered TiN thin films on sapphire and quartz substrates before and after 5 MeV electron irradiation with a fluence of 7×10^{13} e/cm^2. Structural, morphological, optical, and electrical properties were analyzed to observe the impact of electron irradiation on the TiN thin films. The results showed improved electrical properties of the TiN thin films due to high-energy electron irradiation, resulting in increased specific conductivity compared to the as-deposited thin films on both sapphire and quartz substrates. The structural features of the TiN thin films on the sapphire substrate transformed from polycrystalline to amorphous, while the TiN thin films deposited on the quartz substrate remained unchanged. Chemical state analysis indicated changes in the metallic bonding between Ti and N in the deposited TiN on the sapphire substrate, while TiN deposited on the quartz substrate retained its Ti−N bonding. This study provides insights into the effects of electron irradiation on TiN thin films, emphasizing the importance of investigating radiation resistance for the reliable operation of optoelectronic devices and photovoltaic systems in extreme ionizing radiation environments.

INTRODUCTION

Since the first launch of an artificial satellite and the beginning of the space era, the development of space technologies and engineering has led to the creation of numerous applications based on satellite data.[1,2] These applications include communication systems (Internet, mobile phones, radio, and television), global positioning systems (location and navigation services), as well as Earth observation, remote sensing, and monitoring (weather forecasting and disaster warning). The rapid technological advancement in the space industry has created key trends that open up new opportunities for more inclusive prosperity. It is well-known that most satellites and spacecraft operate within the Van Allen belts, which are radiation regions surrounding the Earth, containing high concentrations of energetic charged particles such as electrons and protons.[3,4] The radiation exposure from these charged particles in the belts can damage critical components of spacecraft and satellites, including their optoelectronic devices.[2,5−9] Consequently, due to the intensive development of the space industry and the effects of space radiation, there is a growing need for new radiation-resistant functional electronic and optoelectronic materials.

Prolonged exposure to ionizing radiation negatively affects functional semiconductor materials used in optoelectronic devices and limits their lifespan.[10] Radiation can cause the breaking of chemical bonds within the material and alter its morphological and structural characteristics. Undesirable phenomena such as swelling, polymerization, corrosion, loss of quality, cracking, and other changes in mechanical, optical, and electronic properties can occur.[11] In semiconductor materials, ionizing radiation generates excessive nonequilibrium electron−hole pairs that disrupt the normal operation of electronic and optoelectronic devices, altering their electrical

Received: September 15, 2023
Revised: October 30, 2023
Accepted: December 1, 2023
Published: December 22, 2023

https://doi.org/10.1021/acsomega.3c07053
ACS Omega 2024, 9, 925−933

properties and characteristics.[5,12] Additionally, radiation can lead to charge trapping in oxide layers and interface states of semiconductor devices, altering the distribution of the electric field and causing unwanted noise, thus reducing device functionality.[10] High-energy particles induce atomic displacements in the material's lattice, leading to lattice defects and damage, disrupting the flow of charge carriers, and causing irreversible damage.[13] Ionizing radiation also results in increased leakage currents in semiconductor devices, which can lead to errors, malfunctions, or complete device failure.[10,13,14]

In a low Earth orbit, ionizing radiation mainly consists of electrons and protons, encompassing energies ranging from approximately 100 keV to greater than 10 MeV, with different fluxes up to 10^9 particles/cm^2. Based on the data depicting the worst-case scenarios for various averaging periods, the electron energy interval spans from <200 keV and can extend to 8 MeV, coupled with a dose within the range of 10^3−10^9 electrons/cm^2.[13,15] In specific scenarios, the electron dose may even reach 10^{16} electrons/cm.[2,10,13,15] Meanwhile, proton energies span from a few keV to 100 MeV, accompanied by a dose of $10^{12,13}$ protons/cm^2.[13] The predominant space weather threat to spacecraft in terms of cumulative damage effects originates from trapped electrons rather than solar protons.[16] Hence, comprehending the impact and finding ways to mitigate the effects of electrons and protons on semiconductor materials and devices become crucial elements for successful space exploration and the reliable operation of satellites in low Earth orbit.[2,10,13,16,17]

Presently, there are ongoing efforts to develop various radiation-resistant devices[6,18−24] and investigate the impact of ionizing radiation on material properties for practical applications in the space industry.[17,20,25−31] Titanium nitride (TiN) stands out as a preferred and promising candidate for creating radiation-resistant optoelectronic devices in the space industry.[18,26,27,32,33] TiN boasts exceptional structural, thermal, chemical, electrical, optical, and mechanical properties, along with a wide band gap, making it successfully applicable in various fields of mechanical and electrical engineering.[18,26,34,35] Accordingly, thin films of TiN can be used as conductive transparent layers in heterostructures, photodetectors, light-emitting diodes, and solar cells.[18,36−42]

Furthermore, TiN ceramics have demonstrated remarkable radiation resistance when exposed to argon ions with an energy of 100 keV and a high dose of 3×10^{17} ions/cm^2.[43,44] These results underscore its potential for enhancing the safety of nuclear power plants and finding applications in nuclear reactors. Moreover, it is worth mentioning that thin films of TiN exhibit outstanding radiation resistance when subjected to ionizing radiation with energies in the range of a few hundred keV and high doses in the range of 10^{12-17} ions/cm^2 while retaining their structural, mechanical, electrical, and optical properties.[26,44,45]

It is important to highlight that the majority of studies investigating the radiation resistance of TiN have primarily focused on proton (ion) irradiation.[26,44,45] However, for a comprehensive understanding of radiation effects in Van Allen belts, it is crucial to conduct a detailed investigation into the impact of electronic irradiation on the TiN material. This study delved into the influence of high-energy electrons on the structural, electrical, and optical properties of TiN thin films deposited on sapphire and quartz substrates, which exhibit distinct properties due to their different crystalline structures. Notably, the distribution of electron energy loss in TiN is influenced by properties such as the substrate density, crystalline structure, and electron energy. For this research, an electron fluence of 7×10^{13} e/cm^2 and an energy of 5 MeV were used which correlates with the standard requirements for qualification and quality experience of space solar elements (AIAA S-111).[46] To comprehensively study the structural, morphological, optical, and electrical properties of TiN thin films on quartz and sapphire substrates, various state-of-the-art material characterization techniques were employed both before and after the electronic irradiation process.

EXPERIMENTAL SECTION

TiN Thin Film Deposition. The quartz and sapphire [*c*-(0001)] substrates were sequentially cleaned in acetone, isopropyl alcohol, and ethyl alcohol for 10 min in an ultrasonic bath. Then, the samples were dried with a nitrogen gun. TiN thin films were deposited on sapphire and quartz substrates by the DC reactive magnetron sputtering technique at the following set of parameters: magnetron power 120 W, sample holder temperature 300 °C, deposition time 10 min, argon pressure 2.4×10^{-3} mbar, and nitrogen pressure 4.8×10^{-3} mbar.

Electron Irradiation. The electron linear accelerator ILU-10 at the Institute of Nuclear Physics in Almaty, Kazakhstan was utilized to irradiate with an electron energy of 5 MeV (total fluence of 7×10^{13} e/cm^2). GEZ B6001 polystyrene calorimeters and GEX B3002 film dosimeters measure high-energy electrons' absorbed doses.

Material Characterization Techniques. A high-resolution X-ray diffractometer (SmartLab, Rigaku) was used to measure the crystalline structure of the thin film using Cu $K_{\alpha 1}$ monochromatic radiation at a wavelength of 1.54 Å. Grazing incident X-ray diffraction (GIXRD) was employed as a surface-sensitive diffraction technique to identify the structure of thin film materials. The background was subtracted from all the measured XRD patterns of the TiN thin films. As the GIXRD technique was applied at a 0.5° angle, the beam from GIXRD reached only TiN with a thickness of 90 nm, and no peaks from the substrate were observed. A 2-theta scan was performed using the GIXRD mode in parallel beam configuration with a 1°/min scan speed. The chemical composition of the TiN thin films was measured by X-ray Photoelectron Spectrometer (NEXSA, Thermo Scientific) with a low-power Al Ka X-ray monochromatic source of 1486.9 eV. Ultraviolet photoelectron spectroscopy (UPS) (NEXSA, Thermo Scientific) was employed to accurately measure the work function. The surface of the TiN thin films was etched by Ar ions with an energy of 500 eV for 10 s before X-ray photoelectron spectroscopy (XPS) measurements. The Avantage software from Thermo Scientific Company was used for further analysis of the XPS data. The surface roughness of thin films was measured using an atomic force microscope SmartSPM 1000. The thickness of the films and their surface morphology were inspected using a scanning electron microscope Crossbeam 540. The optical properties of the TiN thin films were investigated by the spectroscopic ellipsometry (SE) technique (SENResearch 4.0 Sentech) in the range of 200−2500 nm with four incidence angles (40, 45, 50, and 55) and wavelength intervals of 1.156 nm. The electrical properties and Hall effect in the thin films were measured using the van der Pauw four-probe method (HMS-5500 Ecopia).

https://doi.org/10.1021/acsomega.3c07053
ACS Omega 2024, 9, 925−933

RESULTS AND DISCUSSION

The sputtered TiN thin films on the *c*-(0001) plane sapphire and quartz substrates have a thickness of approximately 90 nm.

To investigate the effect of electron irradiation on the crystalline structure of the TiN thin films, diffraction pattern measurements were performed using the GIXRD system before and after irradiation. The as-deposited TiN thin films on *c*-(0001) plane sapphire substrates displayed a polycrystalline structure with (111), (200), (220), and (222) planes, consistent with JCPDS card 01-087-0627,[47] as shown in Figure 1. However, after electron irradiation, the structure of TiN thin

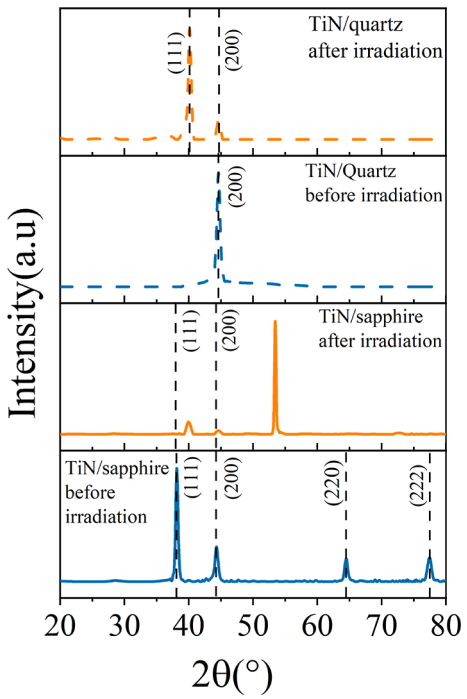

Figure 1. GIXRD measurements of the TiN thin films on quartz and sapphire substrate: before and after irradiation.

films on sapphire transformed into an amorphous structure (Figure 1). The observed peak around 53° in the XRD pattern can be associated with various crystallographic phases, and two possible candidates are hexagonal close-packed (hcp) Ti (COD ID 9011600) and anatase (015) Ti oxide (ICSD: 172914). The appearance of this peak after electron irradiation can be explained by structural changes induced by the high-energy electron bombardment. Electron irradiation can cause lattice defects, disordering, and even phase transformations in materials. For example, in the case of TiN, electron irradiation may induce crystallographic disorder or create vacancies and interstitials in the lattice, which can alter the XRD pattern and result in the appearance of new peaks.

Regarding the as-deposited TiN thin films on quartz, only the (200) plane was observed, in accordance with previous reports.[48,49] After irradiation, the diffraction patterns of the TiN thin films on quartz showed a characteristic peak at 44°,[48−51] identified as the (200) plane,[48−51] but with lower intensity than the as-deposited TiN thin films on quartz (Figure 1). Interestingly, the irradiated TiN thin films on quartz reveal a peak with a high intensity at 40°, identified as the (111) plane.

The change of texture and shift of the diffraction angles exhibited by TiN on quartz and sapphire substrates after the irradiation process finds its explanation in the degree of disorder before and after irradiation.[52] The varied change of texture and shift of the diffraction angles arise due to constraints inherent in the thin film fabrication process, which exert an impact on the thin films' grain size and crystallinity. Notably, the pre-irradiation levels of disorder in TiN thin films deposited on quartz and sapphire differ, primarily attributed to distinct grain sizes calculated across different planes.

The calculation of grain size based on GIXRD patterns of the TiN thin films on both substrates revealed an increase in grain size after irradiation (Table S1 in the Supporting Information). The impact of an increase in grain size following high-energy electron irradiation largely depends on the phase transformation of both crystalline and amorphous phases due to the electron knock-on process.[53] During the knock-on process, there is a creation of an electrostatic force, which is generated by the polarization of atoms and ions under electron irradiation. This, in turn, leads to the motion of free atoms and ions, which contributes to the absorption and dissolution of nanograins.[54] The size of the grains continues to grow. One of the main results of this type of irradiation is an increase in entropy and a shift in Gibbs free energy, which can lead to an irradiation-induced change of texture and shift of the diffraction angles, as noted in previous works.[35]

The changes in the surface roughness of the TiN thin films were monitored by using AFM topography measurements. The RMS roughness values were determined using a discrete approximation method.[55] After irradiation, the RMS value of the TiN films deposited on quartz increased, as seen in Figure 2a,b. Conversely, the TiN thin films deposited on sapphire exhibited a higher range of surface roughness, as shown in Figure 2c,d. Additional top images of the TiN thin film surface captured by SEM can be found in Figure S2 of the Supporting Information. Notably, the SEM images revealed no visible changes on the surface of the thin films.

To further explore the effect of high-energy electron irradiation on the chemical composition of TiN, XPS analysis was performed. Prior to measurements, the surfaces of all TiN thin films were cleaned by using the argon ion etching process to eliminate surface contaminations. The XPS Ti 2p spectra showed two pairs of Ti $2p_{3/2}$ and Ti $2p_{1/2}$ spin−orbit splittings, around 5.9 ± 0.1 eV, in all specimens. The Ti 2p XPS spectra were identified with respect to chemical bonding as Ti−N (454.9 and 460.8 eV), Ti−O−N (456.8 and 462.5 eV), and Ti−O (456.3 and 464.0 eV). The Ti 2p XPS measured spectra were fitted based on the mentioned electron binding energy values. Figure 3 reveals the Ti 2p XPS spectra before and after irradiation on sapphire and quartz substrates. The TiN thin films deposited on quartz and sapphire substrates before irradiation showed Ti $2p_{3/2}$ peaks at 454.9 and 454.7 eV, respectively (Figure 3a,c), associated with Ti−N bonding. As reported in works,[47,56] shakeup peaks at 462.5 eV (Ti−O−N) and 460.8 eV (Ti−N) arise due to broad Ti 3d−N 2p hybridized states located near the Fermi level that relax selection rules, permitting multiple transitions to different states. Under high electron irradiation, the binding energy of the Ti $2p_{3/2}$ doublet shifted to 455.4 eV for the TiN thin films deposited on sapphire and 454.6 eV for TiN thin films deposited on quartz, with full width at half-maximum (fwhm) values of 2.6 and 2.4, respectively (Figure 3b,d). Additionally,

https://doi.org/10.1021/acsomega.3c07053
ACS Omega 2024, 9, 925−933

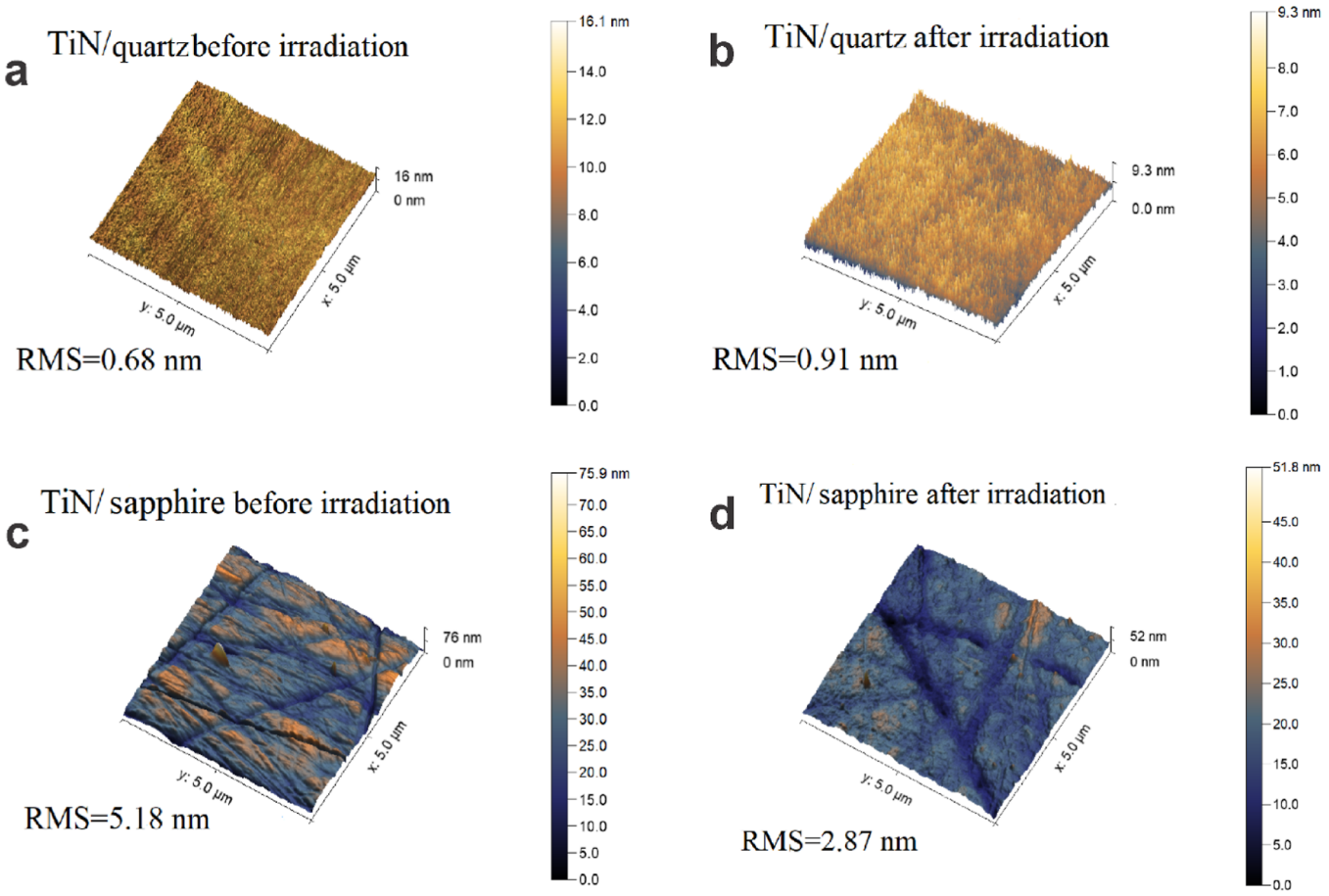

Figure 2. Surface morphology measured by AFM: TiN thin films on quartz before irradiation (a) and after irradiation (b) and TiN thin films on sapphire before irradiation (c) and after irradiation (d).

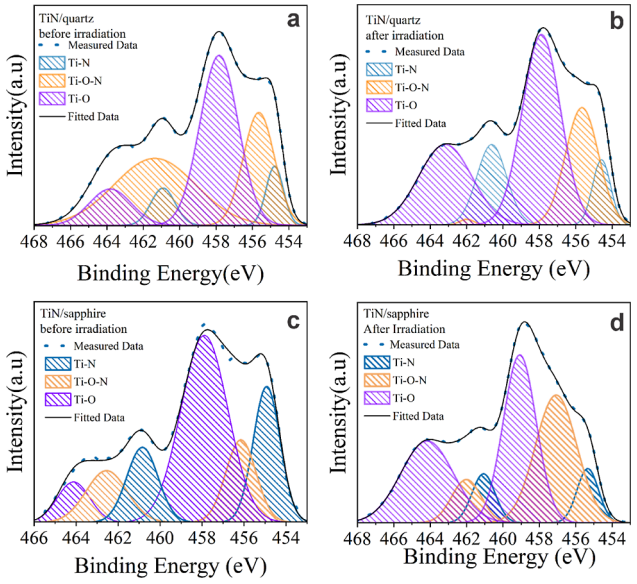

Figure 3. XPS spectra of Ti 2p (a) TiN on quartz as deposited, (b) TiN on quartz after irradiation; (c) TiN on sapphire as deposited, and (d) TiN on sapphire after irradiation.

changes in the relative intensity of Ti 2p peaks were observed in all specimens, which are associated with the change in the crystal structure.[56] Based on the Ti $2p_{3/2}$ and Ti $2p_{1/2}$ peak analysis after electron irradiation, we observed the transformation of Ti−N bonding to Ti−O in the case of the TiN thin films on sapphire. However, electron irradiation affected the TiN thin films deposited on quartz by transforming chemical bonds from Ti−N and Ti−O to Ti−O−N, as shown in Figure 3a,b. This observation can be attributed to a complex process, involving electrochemical interactions between electrons and constituent atoms, as well as the exchange of subsurface nitrogen with oxygen adatoms.[53,57,58]

The work function of the TiN thin films on both types of substrates before and after electron irradiation was determined by employing the UPS technique (Figure 4a). Specifically, the work function was calculated using the onset position in the UPS spectra (see Figure 4b,c).[37] The UPS spectra of the TiN thin films on sapphire before irradiation displayed a cutoff energy higher than that of the TiN on quartz before irradiation, TiN on quartz after irradiation, and TiN on sapphire after irradiation. Moreover, the intensity of the UPS spectra of the TiN thin films after irradiation on both substrates was twice as high as that before irradiation. Figure 4c also revealed a broad defect band in the UPS spectrum of the TiN thin films on both substrates, known to represent a high density of the localized states below the Fermi level, according to previous studies.[58] It is important to note that the density of interface states and Fermi-level pinning can influence band alignment, as mentioned in previous research.[40] As seen in Figure 4d, the as-deposited TiN thin films on sapphire and quartz showed the same work function of slightly above 4.2 eV. However, after electron irradiation, the work function decreased to 4.05 eV.

https://doi.org/10.1021/acsomega.3c07053
ACS Omega 2024, 9, 925−933

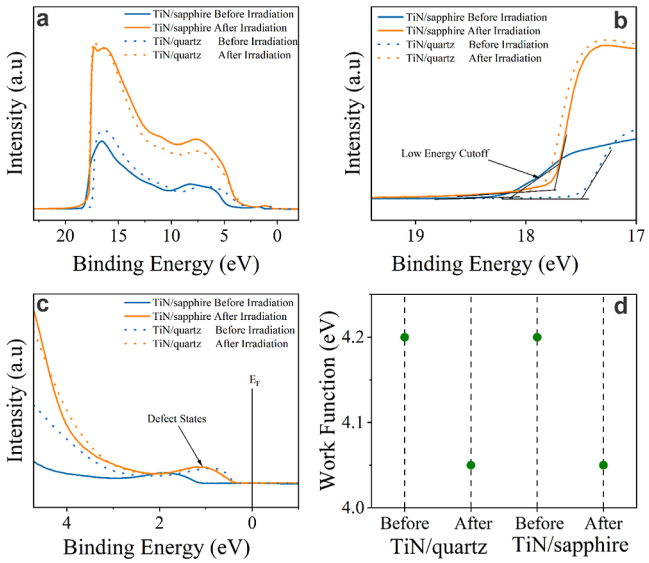

Figure 4. UPS spectra of the TiN thin films on quartz and sapphire before and after irradiation: (a) UPS spectra, (b) UPS spectra of low energy cutoff, and (c) UPS spectra with indicated Fermi level. (d) Comparative analysis of work function.

This reduction is attributed to changes in the density of free charge carriers and surface dipoles, as reported in earlier studies.[37]

The van der Pauw technique was applied to analyze the effect of electron irradiation on the electrical properties of the TiN thin films, enabling the calculation of various parameters such as charge carrier density, specific conductivity, and Hall mobility. Figure 5 displays the electrical properties of the TiN thin films on various substrates before and after exposure to

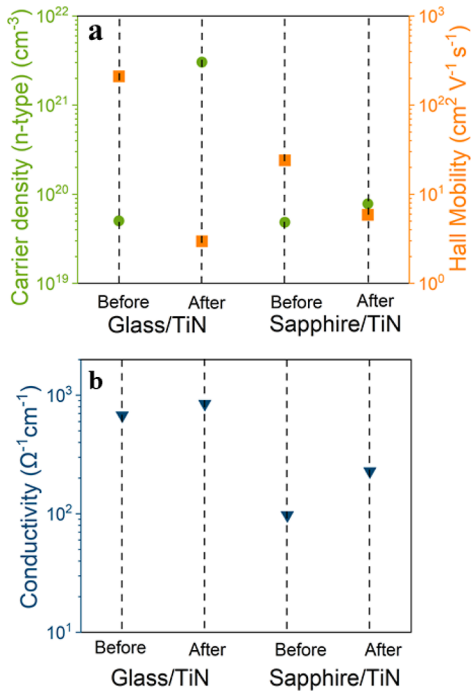

Figure 5. (a) Electron density and their hall mobility for the TiN thin films on quartz and sapphire before and after irradiation. (b) Specific conductivity of the TiN thin films on quartz and sapphire before and after irradiation.

electron irradiation. TiN possesses both metallic and covalent Ti−N bonding,[59] and its unique electrical properties are partially due to the high concentration of free electrons in the conduction band, thermally activated from energy levels associated with excess Ti atoms.[60] The conductivity of TiN thin films comes from unbounded electrons of Ti orbitals.[61] The crystallinity of TiN thin films determines the electrical properties such as resistivity, which is affected by the grain size and grain boundaries. Table 1 in the Supporting Information shows that the grain size of TiN thin films deposited on quartz is lower than that of TiN thin films on sapphire. Thus, the single-crystalline structure substrate serves better as a substrate for TiN thin film's electrical properties.[61,62]

All TiN samples in the study exhibited n-type charge carriers, as indicated by the measured Hall coefficients, as shown in Figure 5a. Comparing the charge carrier density in the TiN thin films on quartz before and after irradiation, an increase by 2 orders of magnitude was observed (Figure 5a). The charge carrier density in the TiN thin films on sapphire substrates also increased slightly under the influence of electron irradiation. As previous research has shown,[63] the charge carrier concentration and mobility are inversely related in TiN thin films, and it was found that the mobility of electrons in the TiN thin films on both substrates decreased after irradiation. Notably, the mobility of electrons in the TiN films on quartz substrates decreased by 2 orders of magnitude after irradiation (Figure 5a). The specific conductivity of the TiN thin films on quartz substrates slightly increased, whereas the TiN thin films on sapphire improved from 97 to 228 Ω^{-1} cm^{-1} after irradiation, as shown in Figure 5b. It is known that the change in specific conductivity of electron-irradiated thin film materials depends on the electron energy and fluence.[44]

SE was employed to measure the refractive index and extinction coefficient of the TiN thin films and their changes after electron irradiation. The Phi and Delta functions obtained from SE measurements were then fitted by using combined models of Drude and Lorentz. The Drude dispersion model accounts for free charge carriers, while the Lorentz dispersion model characterizes bound carrier oscillators.[64]

The refractive index and extinction coefficient of the TiN thin films on both types of substrates were determined through a fitting process (Figure 6a,b). At the range of 3−4 eV, the refractive index of the as-deposited TiN thin films on sapphire was found to be higher than that after electron bombardment. In the remaining ranges (0.6−3 eV) and (4.9−6.5 eV), the refractive index of the TiN thin films on sapphire after irradiation remained higher than that of the as-deposited TiN thin films (Figure 6b). However, for the TiN thin films deposited on quartz, the maximum peak of the refractive index shifted from 3.45 eV for the as-deposited state to 2.85 eV after high-energy electron irradiation (Figure 6a). Additionally, we observe that the refractive index of the TiN on quartz at 0.6−3 and 3.2−6.5 eV ranges is lower than in as-deposited TiN thin films. Meantime, TiN thin film deposited on both substrates reveals the peak of the refractive index at the visible range, which serves as an identification of metallic behavior. It should be noted that a low refractive index of TiN thin films after irradiation enables them to absorb comparatively more photons.

Surprisingly, the extinction coefficient of the TiN thin films deposited on quartz reveals a significant increase after irradiation in the high photon energy region due to the phase transformation of the TiN thin films (Figure 6a).

https://doi.org/10.1021/acsomega.3c07053
ACS Omega 2024, 9, 925−933

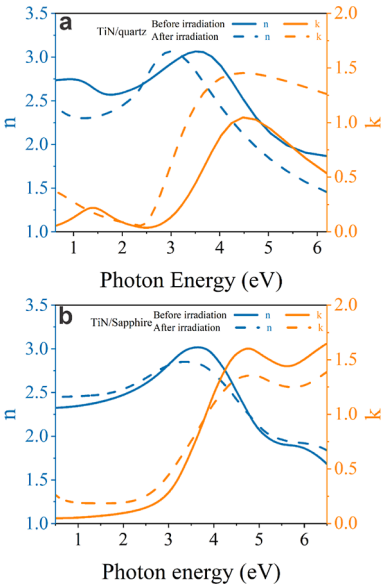

Figure 6. (a) Refractive index (n) and extinction coefficient (k) of TiN thin films on quartz before and after irradiation. (b) Refractive index (n) and extinction coefficient (k) of TiN thin films on sapphire before and after irradiation.

Conversely, the extinction coefficient of the TiN thin films deposited on sapphire was reduced due to electron irradiation, Figure 6b. The modification of the optical properties of the TiN thin films is determined as the development of the electronic structure of the TiN. In principle, the optical properties of the thin film were defined as the interaction of incident light with the thin film expressed in electronic transitions as intraband and interband.[65] The specific form of the extinction coefficient of the TiN at the visible range was determined as interband transition identified as an increase of titanium d-states and nitrogen p-states.[65] Despite the change in the value of the extinction coefficient after electron bombardment, the specific form identified as metallic behavior in TiN thin films deposited on both substrates, before and after irradiation, saves the form around 2.7 eV Figure 6a,b.

In order to determine the band gap of the TiN thin films, we calculated the absorption coefficient based on the SE measurements. Tauc plot is represented as the dependence of $(\alpha h\upsilon)^2$ on the incident photon energy, and the extrapolation of the linear region of $(\alpha h\upsilon)^2$ vs $h\upsilon$ dependence to the photon energy axis identifies the value of the band gap. The Tauc plot revealed that the direct energy band gap of the TiN thin films on both substrates is 3.5 eV before irradiation. Because of electron irradiation, the band gap of the TiN thin films slightly drops to 3.4 eV on sapphire and 3.2 eV on quartz (see Figure S3 in Supporting Information).[66]

CONCLUSIONS

In summary, this investigation delved into the effects of high-energy electron irradiation on TiN thin films deposited on sapphire and quartz substrates. The findings unveiled substantial alterations, including a transition from a polycrystalline to an amorphous structure, changes in surface roughness, and modifications in metallic properties of TiN thin films on sapphire upon irradiation. Similarly, a structural change and shift of the diffraction angles were observed in TiN thin films on quartz, while maintaining unchanged surface roughness and compositional characteristics. Moreover, both substrates exhibited enhanced electrical properties in the wake of irradiation. Notably, the specific conductivity of TiN thin films on sapphire experienced a remarkable increase post-irradiation. These findings underscore the decisive role of the substrate in shaping the attributes of TiN thin films when subjected to electron irradiation, carrying pertinent implications for electronic systems in space.

ASSOCIATED CONTENT

Supporting Information

The Supporting Information is available free of charge at https://pubs.acs.org/doi/10.1021/acsomega.3c07053.

SEM images of cross section and top view of TiN thin films; Tauc plots; and table of grain sizes in TiN thin films (PDF)

AUTHOR INFORMATION

Corresponding Author

Viktor V. Brus − *Department of Physics, Nazarbayev University, Astana 010000, Kazakhstan;* orcid.org/0000-0002-3489-1396; Email: vvbrus@gmail.com

Authors

Gulnur Akhtanova − *Department of Physics, Nazarbayev University, Astana 010000, Kazakhstan;* orcid.org/0000-0002-7481-3675

Yerassyl Yerlanuly − *Al-Farabi Kazakh National University, Almaty 050040, Kazakhstan; Kazakh-British Technical University, Almaty 050000, Kazakhstan;* orcid.org/0000-0001-6757-1041

Hryhorii P. Parkhomenko − *Department of Physics, Nazarbayev University, Astana 010000, Kazakhstan;* orcid.org/0000-0001-5358-1505

Mykhailo V. Solovan − *Faculty of Physics, Adam Mickiewicz University, Poznan 61-614, Poland*

Andrii I. Mostovyi − *Department of Physics, Nazarbayev University, Astana 010000, Kazakhstan; Department of Electronics and Energy Engineering, Yuriy Fedkovych Chernivtsi National University, Chernivtsi 58012, Ukraine*

Aliya K. Nurmukhanbetova − *Energetic Cosmos Laboratory, Nazarbayev University, Astana 010000, Kazakhstan*

Alexander V. Kireyev − *Institute of Nuclear Physics, Almaty 050032, Kazakhstan*

Igor V. Danko − *Institute of Nuclear Physics, Almaty 050032, Kazakhstan;* orcid.org/0000-0001-7377-5913

Pavel A. Oreshkin − *Institute of Nuclear Physics, Almaty 050032, Kazakhstan*

Timur K. Zholdybayev − *Institute of Nuclear Physics, Almaty 050032, Kazakhstan; Al-Farabi Kazakh National University, Almaty 050040, Kazakhstan*

Daniyar M. Janseitov − *Institute of Nuclear Physics, Almaty 050032, Kazakhstan; Al-Farabi Kazakh National University, Almaty 050040, Kazakhstan*

Tlekkabul S. Ramazanov − *Al-Farabi Kazakh National University, Almaty 050040, Kazakhstan*

Complete contact information is available at: https://pubs.acs.org/10.1021/acsomega.3c07053

Author Contributions

Gulnur Akhtanova: investigation, visualization, formal analysis, methodology, writing—original draft. **Yerassyl Yerlanuly:**

https://doi.org/10.1021/acsomega.3c07053
ACS Omega 2024, 9, 925−933

formal analysis, methodology, visualization, validation, writing—original draft, writing—review and editing. **Hryhorii P. Parkhomenko, Mykhailo M. Solovan**, and **Andrii I. Mostovyi:** methodology, thin film deposition. **Aliya K. Nurmukhanbetova, Alexander V. Kireyev, Igor V. Danko, Pavel A. Oreshkin, Timur K. Zholdybayev**, and **Daniyar M. Janseitov:** methodology, electron irradiation. **Tlekkabul S. Ramazanov**: funding acquisition. **Viktor V. Brus:** conceptualization, methodology, supervision, funding acquisition, writing—review and editing.

Notes

The authors declare no competing financial interest.

■ ACKNOWLEDGMENTS

The authors thank the Core Facility team at Nazarbayev University for their assistance and support in XPS, UPS, and SEM measurements. V.V.B. thanks Nazarbayev University Collaborative Research Grant (grant no. 11022021CRP1505) and Nazarbayev University Faculty Development Competitive Research Grant (grant no. 11022021FD2915). Y.Y. thanks the Scientific Research Program (grant no. BR18574080) from the Committee of Science of the Ministry of Science and Higher Education of the Republic of Kazakhstan.

■ REFERENCES

(1) *Handbook of Satellite Applications*; Pelton, J. N., Madry, S., Camacho-Lara, S., Eds.; Springer New York: New York, NY, 2013..

(2) Verduci, R.; Romano, V.; Brunetti, G.; Yaghoobi Nia, N.; Di Carlo, A.; D'Angelo, G.; Ciminelli, C. Solar Energy in Space Applications: Review and Technology Perspectives. *Adv. Energy Mater.* **2022**, *12* (29), 2200125.

(3) Claudepierre, S. G.; Ma, Q.; Bortnik, J.; O'Brien, T. P.; Fennell, J. F.; Blake, J. B. Empirically Estimated Electron Lifetimes in the Earth's Radiation Belts: Van Allen Probe Observations. *Geophys. Res. Lett.* **2020**, *47* (3), No. e2019GL086053.

(4) Gohl, S.; Bergmann, B.; Kaplan, M.; Nemec, F. Determination of Electron and Proton Fluxes in a Low Earth Orbit with SATRAM and Comparison to EPT Data. In *EGU General Assembly 2022*, 2022;..

(5) Troska, J.; Vasey, F.; Weidberg, A. Radiation Tolerant Optoelectronics for High Energy Physics. *Nucl. Instrum. Methods Phys. Res., Sect. A* **2023**, *1052*, 168208.

(6) Solovan, M. M.; Mostovyi, A. I.; Aidarkhanov, D.; Parkhomenko, H. P.; Akhtanova, G.; Schopp, N.; Asare, E. A.; Nauruzbayev, D.; Kaikanov, M.; Ng, A.; Brus, V. V. Extreme Radiation Resistance of Self-Powered High-Performance $Cs_{0.04}Rb_{0.04}(FA_{0.65}MA_{0.35})_{0.92}Pb(I_{0.85}Br_{0.14}Cl_{0.01})_3$ Perovskite Photodiodes. *Adv. Opt. Mater.* **2023**, *11* (10), 2203001.

(7) Sittimart, P.; Ohmagari, S.; Umezawa, H.; Kato, H.; Ishiji, K.; Yoshitake, T. Thermally Stable and Radiation-Proof Visible-Light Photodetectors Made from N-Doped Diamond. *Adv. Opt. Mater.* **2023**, *11* (12), 2203006.

(8) Yang, Y.; Zhu, H.; Wang, L.; Jiang, Y.; Wang, T.; Liu, C.; Li, B.; Tang, W.; Wu, Z.; Yang, Z.; Li, D. In-Depth Investigation of Low-Energy Proton Irradiation Effect on the Structural and Photoresponse Properties of ε-Ga2O3 Thin Films. *Mater. Des.* **2022**, *221*, 110944.

(9) Aglietti, G. S. Current Challenges and Opportunities for Space Technologies. *Front. Space Technol.* **2020**, *1*, 1.

(10) Baker, D. N.; Erickson, P. J.; Fennell, J. F.; Foster, J. C.; Jaynes, A. N.; Verronen, P. T. Space Weather Effects in the Earth's Radiation Belts. *Space Sci. Rev.* **2018**, *214* (1), 17.

(11) Klopotov, A.; Kakushkin, Y.; Potekaev, A.; Volokitin, O.; Kislitsyn, S.; Kulagina, V. Effect Of Irradiation With Low-Energy Alpha Particles On The Structural-Phase State Of Coatings Of Triple Nitride Systems Based On Titanium And Vanadium On Steel. In *2020 7th International Congress on Energy Fluxes and Radiation Effects (EFRE)*; IEEE: Tomsk, Russia, 2020; pp 993−997..

(12) Gohl, S.; Bergmann, B.; Pospisil, S. Design Study of a New Miniaturized Radiation Monitor Based on Previous Experience with the Space Application of the Timepix Radiation Monitor (SATRAM). In *2018 IEEE Nuclear Science Symposium and Medical Imaging Conference Proceedings (NSS/MIC)*; IEEE: Sydney, Australia, 2018; pp 1−7..

(13) Hands, A. D. P.; Ryden, K. A.; Meredith, N. P.; Glauert, S. A.; Horne, R. B. Radiation Effects on Satellites During Extreme Space Weather Events. *Space Weather* **2018**, *16* (9), 1216−1226.

(14) Hastings, D.; Garrett, H. B. *Spacecraft-Environment Interactions*, 1st ed.; *Cambridge atmospheric and space science series*; Cambridge University Press: Cambridge, 2004.

(15) Fennell, J. F.; Claudepierre, S. G.; Blake, J. B.; O'Brien, T. P.; Clemmons, J. H.; Baker, D. N.; Spence, H. E.; Reeves, G. D. Van Allen Probes Show That the Inner Radiation Zone Contains No MeV Electrons: ECT/MagEIS Data. *Geophys. Res. Lett.* **2015**, *42* (5), 1283−1289.

(16) Li, P.; Dong, H.; Lan, J.; Bai, Y.; He, C.; Ma, L.; Li, Y.; Liu, J. Tolerance of Perovskite Solar Cells under Proton and Electron Irradiation. *Materials* **2022**, *15* (4), 1393.

(17) Yerlanuly, Y.; Zhumadilov, R. Y.; Danko, I. V.; Janseitov, D. M.; Nemkayeva, R. R.; Kireyev, A. V.; Arystan, A. B.; Akhtanova, G.; Vollbrecht, J.; Schopp, N.; Nurmukhanbetova, A.; Ramazanov, T. S.; Jumabekov, A. N.; Oreshkin, P. A.; Zholdybayev, T. K.; Gabdullin, M. T.; Brus, V. V. Effect of Electron and Proton Irradiation on Structural and Electronic Properties of Carbon Nanowalls. *ACS Omega* **2022**, *7* (51), 48467−48475.

(18) Solovan, M. M.; Mostovyi, A. I.; Parkhomenko, H. P.; Kaikanov, M.; Schopp, N.; Asare, E. A.; Kovaliuk, T.; Veřtát, P.; Ulyanytsky, K. S.; Korbutyak, D. V.; Brus, V. V. A High-Detectivity, Fast-Response, and Radiation-Resistant TiN/CdZnTe Heterojunction Photodiode. *Adv. Opt. Mater.* **2023**, *11* (2), 2202028.

(19) Farzana, E.; Chaiken, M. F.; Blue, T. E.; Arehart, A. R.; Ringel, S. A. Impact of Deep Level Defects Induced by High Energy Neutron Radiation in β-Ga2O3. *APL Mater.* **2019**, *7* (2), 022502.

(20) Kanhaiya, P. S.; Yu, A.; Netzer, R.; Kemp, W.; Doyle, D.; Shulaker, M. M. Carbon Nanotubes for Radiation-Tolerant Electronics. *ACS Nano* **2021**, *15* (11), 17310−17318.

(21) Nemirovsky, Y.; Asa, G.; Gorelik, J.; Peyser, A. Recent Progress in N-Type CdZnTe Arrays for Gamma-Ray Spectroscopy. *Nucl. Instrum. Methods Phys. Res., Sect. A* **2001**, *458* (1−2), 325−333.

(22) Del Sordo, S.; Abbene, L.; Caroli, E.; Mancini, A. M.; Zappettini, A.; Ubertini, P. Progress in the Development of CdTe and CdZnTe Semiconductor Radiation Detectors for Astrophysical and Medical Applications. *Sensors* **2009**, *9* (5), 3491−3526.

(23) Yun, K.; Lee, T.; Kim, S.; Kim, J.; Seong, T. Fast and Highly Sensitive Photodetectors Based on Pb-Free Sn-Based Perovskite with Additive Engineering. *Adv. Opt. Mater.* **2023**, *11* (1), 2201974.

(24) Lu, J.; Ye, Q.; Ma, C.; Zheng, Z.; Yao, J.; Yang, G. Dielectric Contrast Tailoring for Polarized Photosensitivity toward Multiplexing Optical Communications and Dynamic Encrypt Technology. *ACS Nano* **2022**, *16* (8), 12852−12865.

(25) Gosciniak, J.; Atar, F. B.; Corbett, B.; Rasras, M. CMOS-Compatible Titanium Nitride for On-Chip Plasmonic Schottky Photodetectors. *ACS Omega* **2019**, *4* (17), 17223−17229.

(26) Kozlovskiy, A. L.; Abdigaliyev, M. B.; Akhtanova, G.; Zdorovets, M. V. Radiation Resistance of Thin TiN Films as a Result of Irradiation with Low-Energy Kr14+ Ions. *Ceram. Int.* **2020**, *46* (6), 7970−7976.

(27) Brus, V. V.; Solovan, M. M.; Schopp, N.; Kaikanov, M.; Mostovyi, A. I. Visible to Near-Infrared Photodiodes with Advanced Radiation Resistance. *Adv. Theory Simul.* **2022**, *5* (3), 2100436.

(28) Tsao, J. Y.; Chowdhury, S.; Hollis, M. A.; Jena, D.; Johnson, N. M.; Jones, K. A.; Kaplar, R. J.; Rajan, S.; Van De Walle, C. G.; Bellotti, E.; Chua, C. L.; Collazo, R.; Coltrin, M. E.; Cooper, J. A.; Evans, K. R.; Graham, S.; Grotjohn, T. A.; Heller, E. R.; Higashiwaki, M.; Islam, M. S.; Juodawlkis, P. W.; Khan, M. A.; Koehler, A. D.; Leach, J. H.; Mishra, U. K.; Nemanich, R. J.; Pilawa-Podgurski, R. C. N.; Shealy, J. B.; Sitar, Z.; Tadjer, M. J.; Witulski, A. F.; Wraback, M.; Simmons, J.

https://doi.org/10.1021/acsomega.3c07053
ACS Omega 2024, 9, 925−933

A. Ultrawide-Bandgap Semiconductors: Research Opportunities and Challenges. *Adv. Electron. Mater.* **2018**, *4* (1), 1600501.
(29) Narayan, J.; Joshi, P.; Smith, J.; Gao, W.; Weber, W. J.; Narayan, R. J. Q-Carbon as a New Radiation-Resistant Material. *Carbon* **2022**, *186*, 253−261.
(30) Simos, N.; Hurh, P.; Mokhov, N.; Snead, M.; Topsakal, M.; Palmer, M.; Ghose, S.; Zhong, H.; Kotsina, Z.; Sprouster, D. J. Low-Temperature Proton Irradiation Damage of Isotropic Nuclear Grade IG-430 Graphite. *J. Nucl. Mater.* **2020**, *542*, 152438.
(31) Esquinazi, P.; Spemann, D.; Schindler, K.; Höhne, R.; Ziese, M.; Setzer, A.; Han, K.-H.; Petriconi, S.; Diaconu, M.; Schmidt, H.; Butz, T.; Wu, Y. H. Proton Irradiation Effects and Magnetic Order in Carbon Structures. *Thin Solid Films* **2006**, *505* (1−2), 85−89.
(32) Bueno, J.; Coumou, P. C. J. J.; Zheng, G.; De Visser, P. J.; Klapwijk, T. M.; Driessen, E. F. C.; Doyle, S.; Baselmans, J. J. A. Anomalous Response of Superconducting Titanium Nitride Resonators to Terahertz Radiation. *Appl. Phys. Lett.* **2014**, *105* (19), 192601.
(33) Zheng, Y.; Wu, P.; Yang, H.; Yi, Z.; Luo, Y.; Liu, L.; Song, Q.; Pan, M.; Zhang, J.; Cai, P. High Efficiency Titanium Oxides and Nitrides Ultra-Broadband Solar Energy Absorber and Thermal Emitter from 200 Nm to 2600 Nm. *Opt Laser. Technol.* **2022**, *150*, 108002.
(34) Solovan, M. M.; Brus, V. V.; Maryanchuk, P. D.; Ilashchuk, M. I.; Rappich, J.; Nickel, N.; Abashin, S. L. Fabrication and Characterization of Anisotype Heterojunctions N-TiN/p-CdTe. *Semicond. Sci. Technol.* **2014**, *29* (1), 015007.
(35) Lu, X.; Wang, G.; Zhai, T.; Yu, M.; Xie, S.; Ling, Y.; Liang, C.; Tong, Y.; Li, Y. Stabilized TiN Nanowire Arrays for High-Performance and Flexible Supercapacitors. *Nano Lett.* **2012**, *12* (10), 5376−5381.
(36) An, S.; Liao, Y.; Kim, M. Flexible Titanium Nitride/Germanium-Tin Photodetectors Based on Sub-Bandgap Absorption. *ACS Appl. Mater. Interfaces* **2021**, *13* (51), 61396−61403.
(37) Yang, X.; Liu, W.; De Bastiani, M.; Allen, T.; Kang, J.; Xu, H.; Aydin, E.; Xu, L.; Bi, Q.; Dang, H.; AlHabshi, E.; Kotsovos, K.; AlSaggaf, A.; Gereige, I.; Wan, Y.; Peng, J.; Samundsett, C.; Cuevas, A.; De Wolf, S. Dual-Function Electron-Conductive, Hole-Blocking Titanium Nitride Contacts for Efficient Silicon Solar Cells. *Joule* **2019**, *3* (5), 1314−1327.
(38) Gou, Y.; Wang, H.; Li, X.; Duan, H.; Yang, S.; Han, D.; Fan, L.; Yang, J.; Yang, L.; Wang, F. Constructing Amorphous Titanium Nitride/Titanium Oxides Hybrid Electron Transporting Layer for Achieving Efficient and Stable Perovskite Solar Cells. *Appl. Surf. Sci.* **2022**, *604*, 154518.
(39) Ji, Y.; Ran, F.; Xu, H.; Shen, W.; Zhang, J. Improved Performance and Low Cost OLED Microdisplay with Titanium Nitride Anode. *Org. Electron.* **2014**, *15* (11), 3137−3143.
(40) Khezripour, Z.; Mahani, F. F.; Mokhtari, A. Performance Improvement of Ultrathin Organic Solar Cells Utilizing Light-Trapping Aluminum-Titanium Nitride Nanosquare Arrays. *Opt. Mater.* **2018**, *84*, 651−657.
(41) Liu, C.-C.; Wang, W.-T.; Houng, M.-P.; Wang, Y.-H.; Chen, S.-M. Titanium Nitride as Spreading Layers for AlGaInP Visible LEDs. *IEEE Photonics Technol. Lett.* **2002**, *14* (12), 1665−1667.
(42) Moskovskikh, D.; Vorotilo, S.; Buinevich, V.; Sedegov, A.; Kuskov, K.; Khort, A.; Shuck, C.; Zhukovskyi, M.; Mukasyan, A. Extremely Hard and Tough High Entropy Nitride Ceramics. *Sci. Rep.* **2020**, *10* (1), 19874.
(43) Xue, J.-X.; Zhang, G.-J.; Guo, L.-P.; Zhang, H.-B.; Wang, X.-G.; Zou, J.; Peng, S.-M.; Long, X.-G. Improved Radiation Damage Tolerance of Titanium Nitride Ceramics by Introduction of Vacancy Defects. *J. Eur. Ceram. Soc.* **2014**, *34* (3), 633−639.
(44) Konusov, F.; Pavlov, S.; Lauk, A.; Kabyshev, A.; Novikov, V.; Gadirov, R.; Tarbokov, V.; Remnev, G. Effect of Short-Pulsed Ion Irradiation on the Optical and Electrical Properties of Titanium Nitride Films Deposited by Reactive Magnetron Sputtering. *Nucl. Instrum. Methods Phys. Res., Sect. B* **2022**, *526*, 51−59.
(45) Komarov, F. F.; Konstantinov, S. V.; Strel'nitskij, V. E.; Pilko, V. V. Effect of Helium Ion Irradiation on the Structure, the Phase Stability, and the Microhardness of TiN, TiAlN, and TiAlYN Nanostructured Coatings. *Tech. Phys.* **2016**, *61* (5), 696−702.
(46) Standard: Qualification and Quality Requirements for Space Solar Cells (AIAA S-111A-2014). *Standard: Qualification and Quality Requirements for Space Solar Cells (AIAAS-111A-2014)*; Qualification and Quality Requirements for Space Solar Panels, Ed.; American Institute of Aeronautics and Astronautics, Inc.: Washington, DC, 2014..
(47) Bricchi, B. R.; Mascaretti, L.; Garattoni, S.; Mazza, M.; Ghidelli, M.; Naldoni, A.; Li Bassi, A. Nanoporous Titanium (Oxy)Nitride Films as Broadband Solar Absorbers. *ACS Appl. Mater. Interfaces* **2022**, *14* (16), 18453−18463.
(48) Grayeli Korpi, A.; Ţălu, Ş.; Bramowicz, M.; Arman, A.; Kulesza, S.; Pszczolkowski, B.; Jurečka, S.; Mardani, M.; Luna, C.; Balashabadi, P.; Rezaee, S.; Gopikishan, S. Minkowski Functional Characterization and Fractal Analysis of Surfaces of Titanium Nitride Films. *Mater. Res. Express* **2019**, *6* (8), 086463.
(49) Yu, J.; Phang, P.; Samundsett, C.; Basnet, R.; Neupan, G. P.; Yang, X.; Macdonald, D. H.; Wan, Y.; Yan, D.; Ye, J. Titanium Nitride Electron-Conductive Contact for Silicon Solar Cells By Radio Frequency Sputtering from a TiN Target. *ACS Appl. Mater. Interfaces* **2020**, *12* (23), 26177−26183.
(50) Fani, N.; Savaloni, H. *Investigation on the Formation of Titanium Nitride Thin Films on 304 Type Stainless Steel Using Plasma Focus Device. *J. Theor. Appl. Phys.* **2012**, *6* (1), 30.
(51) Maarouf, M.; Haider, M. B.; Drmosh, Q. A.; Mekki, M. B. X-Ray Photoelectron Spectroscopy Depth Profiling of As-Grown and Annealed Titanium Nitride Thin Films. *Crystals* **2021**, *11* (3), 239.
(52) Aidhy, D. S.; Zhang, Y.; Weber, W. J. A Fast Grain-Growth Mechanism Revealed in Nanocrystalline Ceramic Oxides. *Scr. Mater.* **2014**, *83*, 9−12.
(53) Murray, K. A.; Kennedy, J. E.; McEvoy, B.; Vrain, O.; Ryan, D.; Cowman, R.; Higginbotham, C. L. The Effects of High Energy Electron Beam Irradiation in Air on Accelerated Aging and on the Structure Property Relationships of Low Density Polyethylene. *Nucl. Instrum. Methods Phys. Res., Sect. B* **2013**, *297*, 64−74.
(54) Dong, Z.; Zhao, C.; Shen, J.; Huang, Y. Direct Evidence of the Dynamic Growth of Nanotwinned Copper Grain upon Electron Beam Irradiation. *Cryst. Growth Des.* **2020**, *20* (10), 6493−6501.
(55) Jiang, N.; Zhang, H. J.; Bao, S. N.; Shen, Y. G.; Zhou, Z. F. XPS Study for Reactively Sputtered Titanium Nitride Thin Films Deposited under Different Substrate Bias. *Phys. B* **2004**, *352* (1−4), 118−126.
(56) Zhang, R.; Ma, Q.-Y.; Liu, H.; Sun, T.-Y.; Bi, J.; Song, Y.; Peng, S.; Liang, L.; Gao, J.; Cao, H.; Huang, L.-F.; Cao, Y. Crystal Orientation-Dependent Oxidation of Epitaxial TiN Films with Tunable Plasmonics. *ACS Photonics* **2021**, *8* (3), 847−856.
(57) Graciani, J.; Fdez Sanz, J.; Asaki, T.; Nakamura, K.; Rodriguez, J. A. Interaction of Oxygen with TiN(001):N↔O Exchange and Oxidation Process. *J. Chem. Phys.* **2007**, *126* (24), 244713.
(58) Roy, M.; Sarkar, K.; Som, J.; Pfeifer, M. A.; Craciun, V.; Schall, J. D.; Aravamudhan, S.; Wise, F. W.; Kumar, D. Modulation of Structural, Electronic, and Optical Properties of Titanium Nitride Thin Films by Regulated In Situ Oxidation. *ACS Appl. Mater. Interfaces* **2023**, *15* (3), 4733−4742.
(59) Peng, J.; Kremer, F.; Walter, D.; Wu, Y.; Ji, Y.; Xiang, J.; Liu, W.; Duong, T.; Shen, H.; Lu, T.; Brink, F.; Zhong, D.; Li, L.; Lee Cheong Lem, O.; Liu, Y.; Weber, K. J.; White, T. P.; Catchpole, K. R. Centimetre-Scale Perovskite Solar Cells with Fill Factors of More than 86 per Cent. *Nature* **2022**, *601* (7894), 573−578.
(60) Solovan, M. N.; Brus, V. V.; Maistruk, E. V.; Maryanchuk, P. D. Electrical and Optical Properties of TiN Thin Films. *Inorg. Mater.* **2014**, *50* (1), 40−45.
(61) Yang, C. L.; Wang, J. N.; Ge, W. K.; Guo, L.; Yang, S. H.; Shen, D. Z. Enhanced Ultraviolet Emission and Optical Properties in Polyvinyl Pyrrolidone Surface Modified ZnO Quantum Dots. *J. Appl. Phys.* **2001**, *90* (9), 4489−4493.

https://doi.org/10.1021/acsomega.3c07053
ACS Omega 2024, 9, 925−933

(62) Rasic, D.; Sachan, R.; Chisholm, M. F.; Prater, J.; Narayan, J. Room Temperature Growth of Epitaxial Titanium Nitride Films by Pulsed Laser Deposition. *Cryst. Growth Des.* **2017**, *17* (12), 6634−6640.
(63) Krylov, I.; Xu, X.; Qi, Y.; Weinfeld, K.; Korchnoy, V.; Eizenberg, M.; Ritter, D. Effect of the Substrate on Structure and Properties of Titanium Nitride Films Grown by Plasma Enhanced Atomic Layer Deposition. *J. Vac. Sci. Technol., A* **2019**, *37* (6), 060905.
(64) Ponon, N. K.; Appleby, D. J. R.; Arac, E.; King, P. J.; Ganti, S.; Kwa, K. S. K.; O'Neill, A. Effect of Deposition Conditions and Post Deposition Anneal on Reactively Sputtered Titanium Nitride Thin Films. *Thin Solid Films* **2015**, *578*, 31−37.
(65) Patsalas, P.; Kalfagiannis, N.; Kassavetis, S. Optical Properties and Plasmonic Performance of Titanium Nitride. *Materials* **2015**, *8* (6), 3128−3154.
(66) Abd El-Fattah, H. A.; El-Mahallawi, I. S.; Shazly, M. H.; Khalifa, W. A. Optical Properties and Microstructure of TiNxOy and TiN Thin Films before and after Annealing at Different Conditions. *Coatings* **2019**, *9* (1), 22.

https://doi.org/10.1021/acsomega.3c07053
ACS Omega 2024, 9, 925−933